JOURNAL OF PROPULSION AND POWER
Vol. 22, No. 5, September–October 2006

Laser Absorption Velocimetry of Plasma Flow in Two-Dimensional Magnetoplasmadynamic Arcjet

Kiyoshi Kinefuchi*
University of Tokyo, Tokyo 113-0033, Japan
Ikkoh Funaki†
Japan Aerospace Exploration Agency, Kanagawa 229-8510, Japan
and
Kyoichiro Toki‡
Tokyo University of Agriculture and Technology, Tokyo 184-8588, Japan

Experimental velocimetry in the discharge chamber of a two-dimensional magnetoplasmadynamic (MPD) arcjet, fabricated for experimental internal flow measurement, was conducted to investigate the acceleration process for hydrogen propellant. In the experiment, we evaluated the neutral atom velocity and the temperature from the laser absorption spectroscopy using a tunable diode laser. The results using two types of anode, a flared-type anode and a converging-diverging (C-D)-type anode, were compared for the case with a discharge current of 13 kA and a mass-flow rate of 0.65 g/s. It was found that a large velocity slip between the ions and the neutrals prevented the acceleration of the neutral particles. This velocity slip is expected to reduce thrust performance because the flow with ion-neutral slip requires additional electric power compared to the flow without velocity slip. The velocity slip was reduced in the case of the C-D anode compared to the flared anode because of strong ion-neutral momentum coupling in the throat region of the C-D anode.

Nomenclature

A	=	molecular weight
B	=	magnetic field
E	=	electric field
e	=	elementary charge
F	=	thrust
g	=	gravity constant
I_{sp}	=	specific impulse
j	=	current density
K	=	kinetic energy (no-slip case)
K_{slip}	=	kinetic energy (slip case)
M	=	Mach number
m_e	=	electron mass
$\dot{m}$	=	mass-flow rate
N_e	=	electron number density
P_a	=	deposited power in the anode
p	=	pressure
Q	=	collision cross section
R	=	gas constant
T	=	temperature
u	=	axial velocity
$u_{exhaust}$	=	mean exhaust velocity
V_s	=	anode sheath voltage
$\Delta\nu$	=	Doppler shift frequency
θ	=	incident angle of the laser to plasma
λ	=	mean free path
λ_0	=	center wavelength of the laser
ν_D	=	FWHM of Doppler broadening
σ	=	electric conductivity
τ	=	mean free time
ϕ	=	work function

Subscripts

a	=	atom
e	=	electron
i	=	ion
n	=	neutral

Received 7 April 2005; revision received 17 September 2005; accepted for publication 2 October 2005.

*Graduate Student, Bunkyo-ku; currently Engineer, Japan Aerospace Exploration Agency, Office of Space Flight and Operations. Senior Member AIAA.

†Associate Professor, Institute of Space and Astronautical Science, Sagamihara. Member AIAA.

‡Professor, Institute of Symbiotic Science and Technology, Koganei-city. Senior Member AIAA.

I. Introduction

FOLLOWING the successful development of low-power thrusters (below 10 kW), scaling up electric propulsion systems toward high power is in progress. For example, a high-power Hall thruster as great as 100 kW has been reported in current research,[1] and an arcjet of 100-kW class has been investigated in some ground experiments.[2] Among them, the highest-power electric propulsion device flew in 2002, which demonstrated a 28-kW-class ammonia arcjet. Although these experiments showed the possibility of high-power Hall or arcjet thrusters, their specific impulses are limited; hence, they are not desirable for some missions. The magnetoplasmadynamic (MPD) arcjet is now gaining renewed interest for high-power missions such as a manned Mars mission and large orbital transfer, which will require high I_{sp} as well as a large thrust-to-power ratio. Before realizing an MPD system, however, low thrust efficiency has to be solved. So far, only lithium propellants seem to break through the low-efficiency problem, but the contamination problem remains. For this reason, other propellants such as argon or hydrogen should be used.[3,4] Thruster optimization has been hindered by the poor understanding of energy loss mechanisms, which have limited improvement efforts to purely empirical approaches.

To address the loss mechanisms, the entire plasma parameters have to be measured in addition to the heat loss to the wall. From the data, energy input into kinetic or thermal energy modes can be discussed. Such discussion is important in evaluating what percentage of electric power was used for kinetic energy, that is, producing thrust, and in discussing a method for further improvement. Expected loss mechanisms to be discussed include 1) frozen flow loss, 2) excessive Joule heating that will not be recovered if an appropriate

nozzle design is not used, 3) instability that will lead to additional heating, and 4) velocity slip (that will cause additional power consumption if only the ions are accelerated.). Some of these issues have been measured in past research, but difficulty in the plasma measurement of the MPD arcjets prevents all of the data from being measured simultaneously. Because such difficulties are always attributed to the difficulty in identifying neutral particle parameters, adopting precise measurement using laser spectroscopy is reasonable.

In this paper, we applied laser absorption diagnostics to the measurement of the atomic flow in the MPD arcjet. We selected a two-dimensional MPD arcjet in quasi-steady operation, for which a lot of plasma as well as magnetic field data will help in understanding the complete flowfield.[5] This is in contrast to past reports, which are limited to the plume measurement of the axisymmetric MPD arcjet.[6–12] In addition, we used one of the most promising gases, hydrogen, as a propellant gas, targeting the most interesting I_{sp} range, 3000–5000 s, for the measurement.

II. Experimental Apparatus and Procedures

A. Two-Dimensional MPD Arcjet

The two-dimensional MPD arcjet (Fig. 1) provides a nearly two-dimensional flowfield with eight discharge channels, each of which has a centered 2% Th-W cathode and two Cu anodes. Two Cu anodes set in one channel were electrically independent in order to achieve uniform discharge. Two types of anode were fabricated, and their geometries are shown in Fig. 2. One is simple flared-type anode, and the other is converging-diverging (C-D)-type anode. The thruster head was placed inside a stainless-steel vacuum tank of 0.8 m in diameter and 2.0 m in length, which was evacuated to less than 2 mPa before each firing.

The fast-acting valve (FAV)[13] allowed us to feed gaseous propellants featuring a rectangular waveform signal. The FAV simultaneously opens and closes eight valves, and the gas in the reservoir flows through the choked orifices of 1.2 mm in diameter. A gas pulse of about 5-ms duration was then introduced into the chamber by eight gas ports located between the anodes and the cathodes.

After the gas pulse reaches its quasi-steady state, the ignition of a pulse-forming network (PFN)[14] is triggered. The PFN supplies the discharge current with a 0.2-ms flat-topped waveform in the quasi-steady mode.[15] All of the performance and plasma parameters were measured during this 0.2-ms quasi-steady-state time interval. Once the PFN is triggered, a charging voltage of at least 2 kV automatically introduces arc breakdown. Channel-to-channel discharge uniformity was achieved by forcing the total discharge current through 16 equally divided resistors. As for the H_2 propellant, the mass-flow rate was controlled by adjusting the reservoir pressure. The average values of the mass-flow rate were confirmed from the rectangular pulse shape determined by the pressure gauge and the measured reduction in the reservoir pressure for several shots. The uncertainty of the mass flow was 5%.

The discharge current was measured using a Rogowski coil with an integrating circuit calibrated with a known shunt resistance. Voltage measurement was performed with a current probe, which detects the small current bled through a known resistor between the electrodes. Major errors in the thrust and in the discharge voltage measurement are caused by shot-to-shot deviations. However, they were less than 5% of the averaged value of more than five shots. As for the total current measurement, such shot-to-shot error was less than 1%.

B. Laser Absorption Spectroscopy

Plasma properties were obtained using laser absorption spectroscopy.[16] The ratio of absorbed laser power can be plotted against the laser wavelength as shown Fig. 3, which includes information on the plasma properties such as plasma velocity, density, and temperature.

When the particle has a velocity component whose direction is the same as the laser path, a Doppler shift corresponding to this velocity takes place. Based on this, the particle velocity is obtained

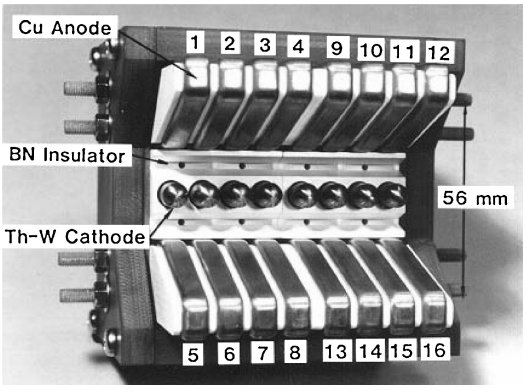

Fig. 1 Photograph of two-dimensional MPD arcjet.

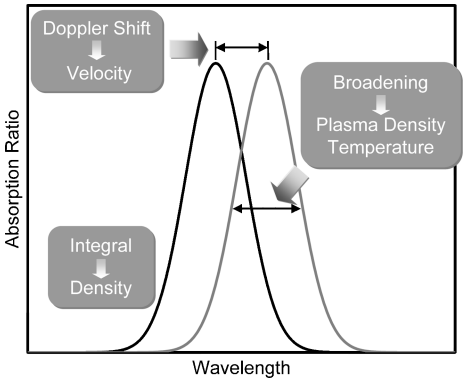

Fig. 3 Relationship between spectrum and plasma parameters.

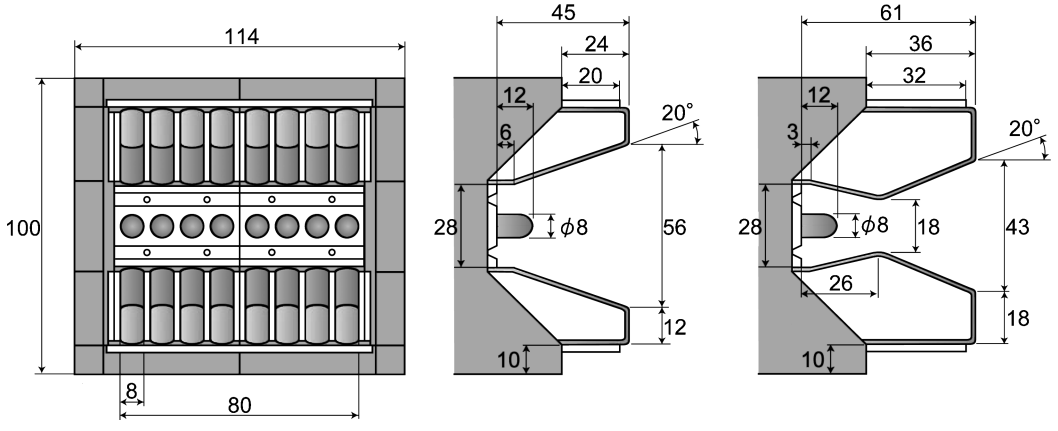

Fig. 2 Geometries of two-dimensional MPD arcjet (unit: mm).

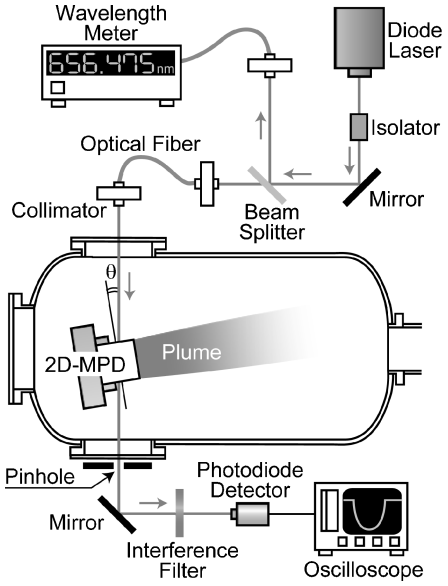

Fig. 4 Laser absorption spectroscopy system.

from this Doppler shift frequency from the following expression:

$$u = \frac{\lambda_0 \Delta \nu}{\sin \theta_1 - \sin \theta_2} \tag{1}$$

The broadening of the spectrum contains information concerning the plasma density[17] and the heavy particle temperature.[18] The heavy particle temperature is shown as follows:

$$T = \frac{A\,(\lambda_0 \nu_D)^2}{8R\,\ell_n 2} \tag{2}$$

Two types of broadening, Doppler broadening and Stark broadening, are separated by fitting a Voigt profile to the spectrum.[18] The integral of the spectrum corresponds to the density of the particle at each energy level.

The laser absorption spectroscopy system is shown in Fig. 4. A semiconductor laser was adopted as the laser source, and the absorption intensity was measured using a photodiode detector. The wavelength of the laser was modulated around 656 nm (Balmer α line of the hydrogen atom). Thus, the atoms are excited from principal quantum number 2 through 3 by the laser beam. The intensity of the incident laser to the two-dimensional MPD is approximately 0.15 mW, and no saturation of laser absorption takes place when sweeping the laser frequency around the Balmer α line. A pinhole (5 mm in diameter) and an interference filter whose wavelength corresponds to the laser frequency are used to remove plasma emissions as thoroughly as possible.

Taking into account the stabilization of the semiconductor laser source, the reproducibility of the absorption spectrum should be estimated to be ± 1 pm for the center wavelength and ± 5 pm for the spectrum broadening determination. Thus, the accuracy of the hydrogen atom velocity and the temperature are approximately ± 1 km/s and ± 0.5 eV, respectively.

To obtain the Doppler shift, the laser beam was directed at incident angle θ relative to the two-dimensional MPD arcjet, as can be seen in Figs. 4 and 5. Comparing the two spectra for incident angles θ_1 and θ_2, the Doppler shift was estimated, and from Eq. (1) the axial velocity was calculated. In this experiment, θ_1 and θ_2 were set at $+10$ and -10 deg, respectively, so that the spectrum is averaged in the 14-mm-wide region shown in Fig. 5.

The measurement points, located at the center of the 14-mm-wide region in Fig. 5, are shown in Fig. 6. Because it was impossible to sweep the laser wavelength in a range wider than the spectrum broadening of hydrogen in the 0.2-ms duration of the discharge, the following procedure was performed: 1) set the laser frequency, 2) firing of the two-dimensional MPD arcjet, 3) acquisition of the absorption intensity, and 4) repetition of steps 1–3 until the spectrum was obtained.

Table 1 Basic performance[19]

Parameter	Flared	C-D
Propellant	H_2	H_2
Mass-flow rate	0.65 ± 0.03 g/s	0.65 ± 0.03 g/s
Discharge current	13.0 ± 0.1 kA	13.0 ± 0.1 kA
Discharge voltage	117 ± 6 V	91 ± 5 V
Thrust	27 ± 1 N	24 ± 1 N
Specific impulse	4200 ± 400 s	3800 ± 400 s
Thrust-to power ratio	18 ± 2 mN/kW	20 ± 2 mN/kW
Efficiency	$37 \pm 11\%$	$38 \pm 11\%$

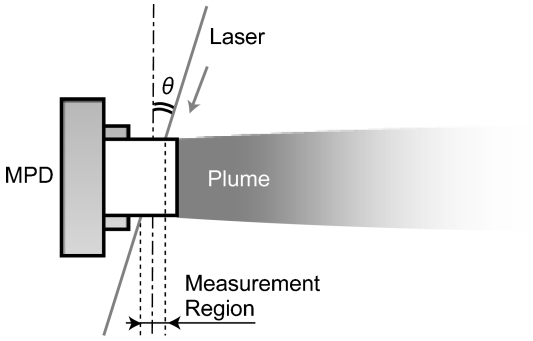

Fig. 5 Incident laser angle for the Doppler shift measurement.

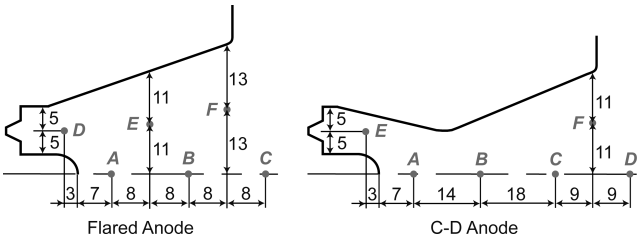

Fig. 6 Measurement points (unit: mm).

III. Experimental Results and Discussion

A. Operational Condition of Two-Dimensional MPD Arcjet

The operational conditions and basic performance of the flared anode and the C-D anode are given in Table 1. The discharge current and the mass-flow rate are the same in both cases. The specific impulse of the flared anode is superior to the C-D anode. However, because the discharge current path in the C-D anode is shorter than that of the flared anode, the discharge voltage is relatively low in the case of the C-D anode such that the thrust efficiencies are almost the same. The discharge current waveform shown in Fig. 7a has approximately 200-μs quasi steady state, and the discharge duration is about 500 μs in the full-width half-maximum. The voltage waveforms of both the flared and the C-D anodes shown in Figs. 7b and 7c also have a quasi steady state. The experimental data given in Table 1 and the absorption ratio were evaluated on quasi-steady duration. Note that although the actual measurements in both this paper and Ref. 19 were taken at identical operating conditions, the authors of Ref. 19 refer to the data using the design values rather than the actual experimental values.

B. Laser Absorption Profiles and Analysis

The laser absorption waveforms of several laser wavelengths are shown in Fig. 7d in the case of the flared anode. These waveforms also have a quasi steady state. By plotting the averaged values of the absorption ratio in this quasi-steady period, the absorption spectrum is obtained as shown in Fig. 8, in which two profiles corresponding to two laser incident angles are shown. A Doppler shift is apparently observed in Fig. 8. The hydrogen-atom axial-velocity distribution calculated from the Doppler shift using Eq. (1) and the atomic temperature evaluated from Eq. (2) are shown in Figs. 9. (flared anode) and 10 (C-D anode). The absorption waveform at point E of the C-D anode was unstable, and reproducibility could not be confirmed, and

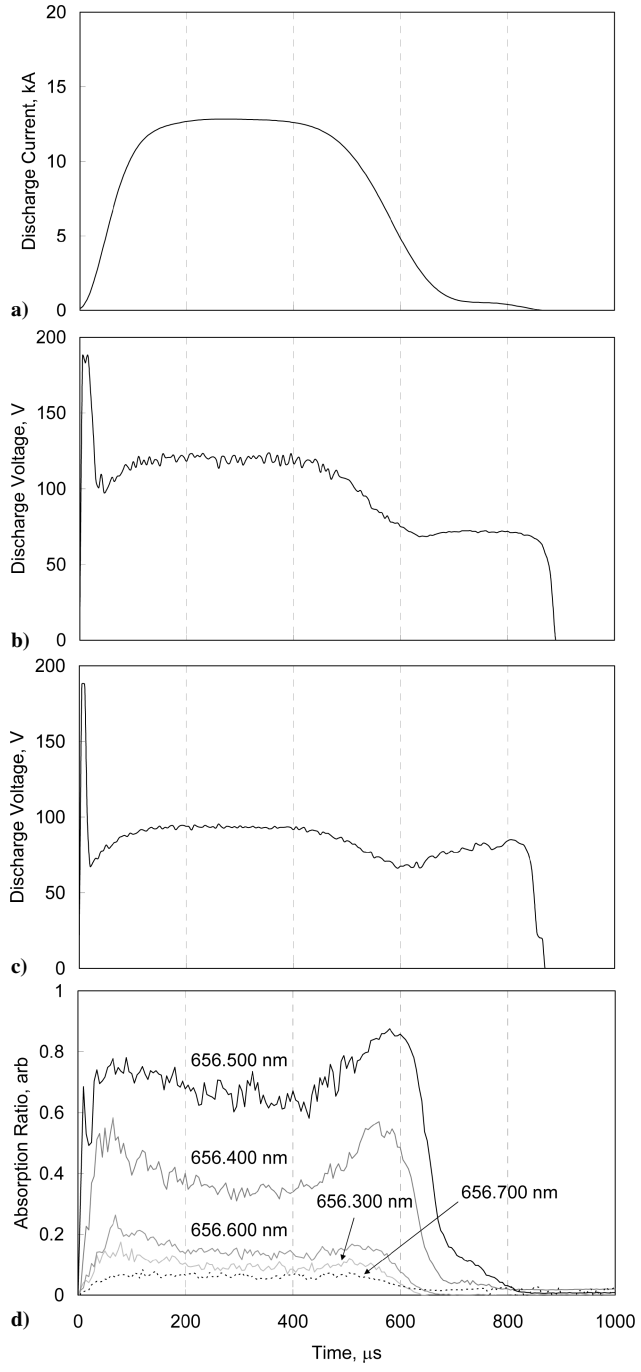

Fig. 7 Waveform examples of the flared anode: a) discharge current, b) discharge voltage of the flared anode, c) discharge voltage of the C-D anode, and d) absorption ratio of the flared anode at point A in Fig. 6.

so the velocity and the temperature are not shown in these figures. Figures 9c and 10c show the atom Mach number calculated by the velocity and the temperature.

C. Acceleration in the Case of the Flared Anode

In the case of flared anode, in the downstream direction the atomic axial velocity decreases as shown in Fig. 9a. The whole flowfield of neutral particles remains subsonic except near the cathode tip as shown in Fig. 9c, where the atom reaches a maximum speed of 20 km/s. To discuss the collisional effect in the discharge chamber, the plasma-density distributions measured using a Mach–Zehnder interferometer are also shown in Figs. 11a and 12a with the discharge current path. In Figs. 11b and 12b, the percentage value for each line corresponds to the amount of current to total current passing through the upstream area of each line. These plasma density

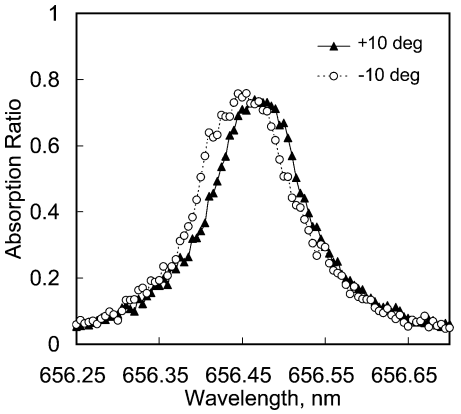

Fig. 8 Absorption spectrum example (measured at flared anode point A).

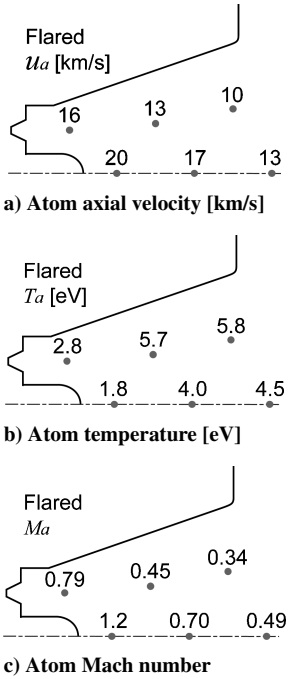

Fig. 9 Atomic velocity, temperature, and Mach number of the flared anode.

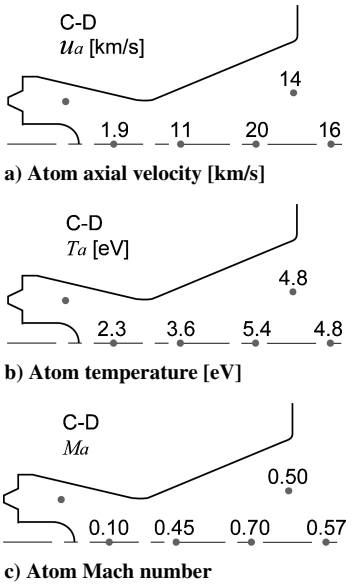

Fig. 10 Atomic velocity, temperature, and Mach number of the C-D anode.

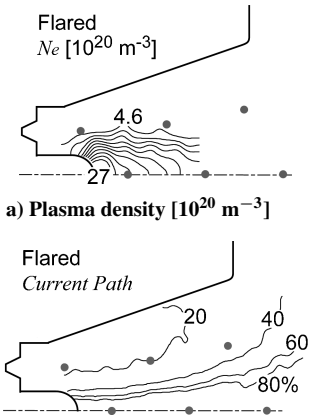

a) Plasma density [10^{20} m^{-3}]

b) Current path

Fig. 11 Plasma density and discharge current path (flared anode).[19]

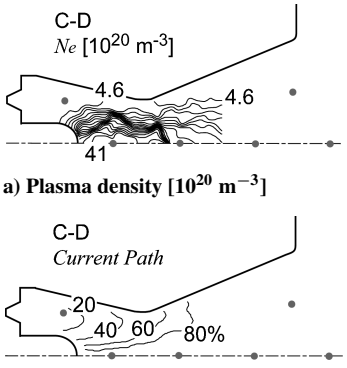

a) Plasma density [10^{20} m^{-3}]

b) Current path

Fig. 12 Plasma density and discharge current path (C-D anode).[19]

distributions and current paths are referred to in Ref. 19. In the vicinity of the cathode tip, a high-plasma-density region appears, as shown in Fig. 11a, and the collision frequency between the ions and neutrals is the highest. Thus, ion momentum is transferred to neutral particles; hence, these neutrals are sufficiently accelerated at the cathode tip. However, except for cathode-tip region the neutrals are affected only by certain aerodynamic mechanisms. Because neutral particle flow is subsonic and the nozzle shape is flared, the neutrals are decelerated. The atomic temperature shown in Fig. 9b also increases in the downstream direction, probably because of an aerodynamic effect.

For detailed discussion on the momentum exchange, the mean free path of atoms against ions is estimated using the following expression:

$$\lambda_{\mathrm{ai}} = 1/Q_{\mathrm{ai}}N_e \tag{3}$$

where $Q_{\mathrm{ai}} = 3.52 \times 10^{-20}$ m^2, and concerning plasma density N_e, the data measured using the Mach–Zehnder interferometer shown in Fig. 11a are applied as for the region where plasma density data are available. The mean free paths of the flared anode and the C-D anode are shown in Fig. 13. Comparing the mean free path of the flared anode with the size of the flared anode, momentum transfer can take place only in the cathode-tip region.

In this experiment, the neutrals did not accelerate but decelerated in the discharge chamber. To compare the velocity by laser spectroscopy with the mean exhaust velocity estimated from the specific impulse, we used the following equation:

$$u_{\mathrm{exhaust}} = I_{\mathrm{sp}}g \tag{4}$$

In this equation, the effect of pressure thrust is ignored. The exhaust velocities are summarized in Table 2. The value of mean exhaust velocity calculated from Eq. (4) is much larger than the exhaust velocity of the atoms. Therefore, at the thruster exit, the ions are

Table 2 Atomic exhaust velocity and estimated mean exhaust velocity

Parameter	Flare	C-D
u_a, km/s	13	16
u_{exhaust}, km/s	42	37

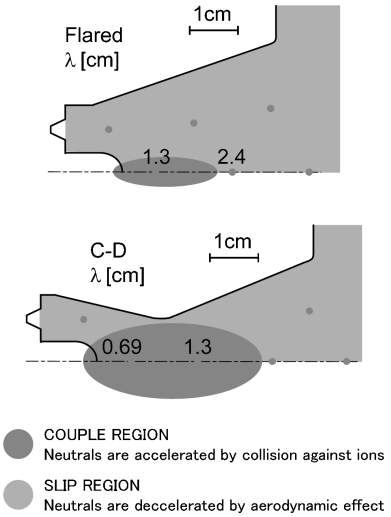

Fig. 13 Mean free path of momentum transfer of atom against ion and summary of acceleration mechanisms.

sufficiently accelerated, but the atoms are not. It is easily explained that this so-called atom-ion velocity slip requires extra power. We will derive a useful equation to evaluate the velocity slip effects to the electric field. The electron momentum equation is expressed as follows:

$$\frac{\nabla p_e}{N_e e} + \boldsymbol{E} + \boldsymbol{u}_e \times \boldsymbol{B} = \frac{m_e}{e\tau_{\mathrm{ei}}}(\boldsymbol{u}_i - \boldsymbol{u}_e) + \frac{m_e}{e\tau_{\mathrm{en}}}(\boldsymbol{u}_n - \boldsymbol{u}_e) \tag{5}$$

Substituting $\boldsymbol{u}_e = \boldsymbol{u}_i - \boldsymbol{j}/eN_e$, we obtain

$$\frac{\nabla p_e}{N_e e} + \boldsymbol{E} + \boldsymbol{u}_i \times \boldsymbol{B} = \frac{\boldsymbol{j}}{\sigma} + \frac{\boldsymbol{j} \times \boldsymbol{B}}{N_e e} + \frac{m_e}{e\tau_{\mathrm{en}}}(\boldsymbol{u}_n - \boldsymbol{u}_i) \tag{6}$$

For example, as for the flared anode at point E in Fig. 6, the electric field is approximately 3 kV/m; this is estimated from the discharge voltage (117 V shown in Table 1) and the discharge current path (Fig. 13b) neglecting the sheath voltage drop. The estimated magnetic field is 0.08 T, which is calculated from expected discharge current density Fig. 11b discharge current path and Ampere's law; assuming 10 to 40 km/s ion velocity at point E, $u_i B$ becomes 1 to 3 kV/m. The electron pressure gradient, the first term on the left-hand side, might be less than 0.2 kV/m. τ_{en} might be greater than 10^{-9} s, and $|\boldsymbol{u}_n - \boldsymbol{u}_i|$ is less than 30 km/s, so that the last term on the right-hand side might be less than 0.2 kV/m. In conclusion, the value of $u_i B$ is comparable to E, and the absolute values of the first term on the left-hand side (the electron pressure gradient) and the last term on the right-hand side could be ignored in comparing $u_i B$ and E.

When only the ions are accelerated, the $\boldsymbol{u}_i \times \boldsymbol{B}$ term in Eq. (6) becomes more negative; thus, in order to keep the discharge current constant, the first term, which corresponds to the required discharge voltage, must increase, and, as a result, extra voltage (hence power) is needed. The component of $\boldsymbol{u}_i \times \boldsymbol{B}$ parallel to $\boldsymbol{E}$ might be comparable to the electric field; thus, the effect of velocity slip to the electric field increase cannot be ignored in our MPD arcjet.

In addition to this extra power requirement, the thrust efficiency is always smaller for a case with velocity slip.[6] If hydrogen atoms and ions are uniformly accelerated and exhausted at the same velocity ($u_i = u_a = u_{\mathrm{exhaust}}$), the thrust power is expressed as follows:

$$K = \tfrac{1}{2}\dot{m}u_{\mathrm{exhaust}}^2 \tag{7}$$

When velocity slip occurs, the thrust power with velocity slip case K_{slip} is greater than that of uniformly accelerated case K for the following reason. If the mass-flow rate and the thrust are the same in both cases, they are expressed as follows:

$$\dot{m} = \dot{m}_i + \dot{m}_a \tag{8}$$

$$F = \dot{m} u_{\text{exhaust}} = \dot{m}_i u_i + \dot{m}_a u_a \tag{9}$$

In Eq. (9) the pressure thrust term is ignored. Using the preceding equations, the relationship between K and K_{slip} is derived as follows:

$$K_{\text{slip}} = \tfrac{1}{2}\dot{m}_i u_i^2 + \tfrac{1}{2}\dot{m}_a u_a^2 \geq K \tag{10}$$

The "equal" sign is valid only when there is no velocity slip. Thus, in a case with velocity slip, extra thrust power is required compared to a case with no slip, even if thrust and mass flow rate are the same. Therefore, the velocity slip causes a decrease in thrust efficiency. In other words, the actual propellant utilization efficiency worsens by this selective acceleration.

The low thrust efficiency of MPD arcjets is a drawback preventing their widespread use in space. This is caused not only by velocity slip but also by extremely high temperature levels, as shown in Fig. 9b. If the ion temperature is equal to the atom temperature, the thermal power to input power ratio is 28% for the flared anode and 38% for the C-D anode. The ion temperature might be greater than the atom temperature; thus, a large thermal energy fraction is expected in the exhaust plume. In addition, as shown in Fig. 9b, the temperature is lowest around the cathode tip, and the reason is that most of the energy is used for excitation and ionization.

Aside from the frozen flow losses discussed so far, a large amount of electrode losses is expected in the discharge chamber of the MPD arcjet.[20,21] The electrode losses are estimated from the anode power deposition, which is calculated as follows:

$$P_a = J(V_s + 5kT_e/2e + \phi) \tag{11}$$

Because V_s, the anode sheath voltage, was not obtained in our experiment, $V_s = 20\ V$ (Refs. 20 and 21) is assumed, then the lost power in the anode sheath is 0.26 MW. Using experimentally obtained electron temperature $T_e = 0.6$ eV[5], the random electron thermal energy, the second term of Eq. (11), is found to be 0.02 MW. From the work function of cupper, $\phi = 4$ V, the last term of the Eq. (11) becomes 0.05 MW. Therefore, P_a is estimated 0.33 MW, and the percentage of P_a to the total input power is approximately 20%.

D. Acceleration in the Case of the C-D Anode

Because there is a converging part for the C-D anode, the flow stagnates near the cathode-tip region, and the discharge current concentrates at the throat-cathode-tip region as shown in Fig. 12b. In this configuration, the high-plasma-density region is large compared to the flared anode case, as shown in Fig. 12a, and the neutrals are accelerated using the energy imparted by the ions via collisional momentum transfer. Further downstream, near the thruster exit, velocity slip starts to occur, and the neutrals are slightly decelerated. This is also proven by the evaluation of the mean free path shown in Fig. 13.

As shown in Table 2, the experimentally measured neutral exhaust velocity in the C-D anode case ($u_a = 16$ km/s) is greater than that of the flared anode case (13 km/s). In the C-D anode case, the difference between the mean exhaust velocity and the atomic exhaust velocity is smaller than that of the flared anode. Therefore, the energy loss caused by velocity slip is reduced for the C-D anode case.

In addition, the extremely high atomic temperature in the whole region and the low temperature in the cathode tip region can be explained using same reasoning as for the flared anode case. Because of this high temperature, the hydrogen atoms in the whole of the C-D anode are subsonic as shown in Fig. 10c. Thus, we can again say that the atoms are accelerated not by its aerodynamic effect but by the momentum transfer from the ions. In Fig. 13, the mean free-path distribution and a schematic illustration are provided to summarize the existing acceleration mechanisms for the two types of anode considered in this study.

IV. Conclusions

Laser absorption spectroscopy was applied for a two-dimensional magnetoplasmadynamic (MPD) arcjet using two types of anode. The atomic velocities were evaluated from the Doppler shift of the laser absorption spectrum, and the experimental results revealed that although the ions were sufficiently accelerated the atoms were not sufficiently accelerated in a relatively large portion of the discharge chamber for 13-kA discharge current and 0.65-g/s mass-flow rate. This can be explained by the fact that the atom-ion collision rate, that is, momentum transfer, is not sufficiently high. This velocity slip will decrease the thrust efficiency. In addition, the measured temperatures were found to be extremely high, and this is considered to be one of the reasons for the low thrust efficiency of the MPD arcjets. Comparing the results for the two different anode configurations, at relatively low I_{sp} operation, 3000–5000 s with moderate ionization rates, the design enabling higher plasma density (conversing-diverging anode) was found to reduce ion-atom velocity slip caused by efficient momentum transfer between atoms and ions.

References

[1] Jacobson, D. T., Manzella, D. H., Hofer, R. R., and Peterson, P. Y., "NASA's 2004 Hall Thruster Program," AIAA Paper 2004-3600, Jan. 2004.

[2] Auweter-Kurtz, M., Gölz, T., Habiger, H., Hammer, F., Kurtz, H., Riehle, M., and Sleziona, C., "High-Power Hydrogen Arcjet Thrusters," *Journal of Propulsion and Power*, Vol. 14, No. 5, 1998, pp. 764–773.

[3] LaPointe, M. R., "High Power MPD Thruster Development at the NASA Glenn Research Center," *Proceedings of 28th International Electric Propulsion Conference* [CD-ROM], March 2003.

[4] Sovey, J. S., and Mantenieks, M. A., "Performance and Lifetime Assessment of Magnetoplasmadynamic Arc Thruster Technology," *Journal of Propulsion and Power*, Vol. 7, No. 1, 1991, pp. 71–83.

[5] Toki, K., Sumida, M., and Kuriki, K., "Multichannel Two-Dimensional Magnetoplasmadynamic Arcjet," *Journal of Propulsion and Power*, Vol. 8, No. 1, 1992, pp. 93–97.

[6] Malliaris, A. C., and Libby, D. R., "Spectroscopic Study of Ion-Neutral Coupling in Plasma Acceleration," *AIAA Journal*, Vol. 9, No. 1, 1971, pp. 160–167.

[7] Jahn, R. G., Clark, K. E., Oberth, R. C., and Turchi, P. J., "Acceleration Patterns in Quasi-Steady MPD Arcs," *AIAA Journal*, Vol. 9, No. 1, 1971, pp. 167–172.

[8] Hoell, J. M., Burlock, J., and Jarrett, O., Jr., "Velocity and Thrust Measurements in a Quasi-Steady Magnetoplasmadynamic Thruster," *AIAA Journal*, Vol. 9, No. 10, 1971, pp. 1969–1974.

[9] Turco, A., Genovesi, G., Paganucci, F., Andrenucci, M., Beverini, N., and Strumia, S., "Tunable Diode Laser Absorption for Argon Plasma Produced in an MPD Thruster," AIAA Paper 94-3298, June 1994.

[10] Sovie, R. J., and Connolly, D. J., "Effect of Background Pressure on Magnetoplasmadynamic Thruster Operation," *Journal of Spacecraft and Rockets*, Vol. 7, No. 3, 1970, pp. 255–258.

[11] Sovie, R. J., and Connolly, D. J., "A Study of Axial Velocities in an Ammonia MPD Thruster," *AIAA Journal*, Vol. 7, No. 4, 1969, pp. 723–725.

[12] Inutake, M., Ando, A., Hattori, K., Tobari, H., and Yagai, T., "Characteristics of a Supersonic Plasma Flow in a Magnetized Nozzle," *Journal of Plasma and Fusion Research*, Vol. 78, No. 12, 2002, pp. 1352–1360.

[13] Suzuki, H., Uematsu, K., and Kuriki, K., "Endurance Test of Fast Acting Valve," AIAA Paper 85-2058, Sept.–Oct. 1985.

[14] Kuriki, K., Gohnai, T., Yoshida, T., Harada, H., Ijichi, K., and Obara, H., "Power Supply for MPD Arcjet," *Proceedings of 17th International Electric Propulsion Conference*, Paper 84-26, 1984, pp. 168–172.

[15] Clark, K. E., and Jahn, R. G., "Quasi-Steady Plasma Acceleration," *AIAA Journal*, Vol. 8, No. 2, 1970, pp. 216–220.

[16] Mellon, M. G., *Analytical Absorption Spectroscopy*, Wiley, New York, 1950.

[17] Griem, H. R., *Spectral Line Broadening by Plasma*, Academic Press, 1974, Chap. 4.

[18] Lochte-Holtgreven, W., *Plasma Diagnostics*, North-Holland Pub., Amsterdam, 1968, Chap. 2 and 5.

[19] Funaki, I., Toki, K., and Kuriki, K., "Electrode Configuration Effect on the Performance of a Two-Dimensional Magnetoplasmadynamic Arcjet," *Journal Propulsion and Power*, Vol. 14, No. 6, 1998, pp. 1043–1048.

[20] Myers, R., Kelly, A. J., and Jahn, R. G., "Electrothermal-Electromagnetic Hybrid Thruster Research," AIAA Paper 87-1018, May 1987.

[21] Gallimore, A. D., Kelly, A. J., and Jahn, R. G., "Anode Power Deposition in Magnetoplasmadynamic Thrusters," *Journal of Propulsion and Power*, Vol. 9, No. 3, 1993, pp. 361–368.